This article has been accepted for publication in IEEE Transactions on Applied Superconductivity. This is the author's version which has not been fully edited and content may change prior to final publication. Citation information: DOI 10.1109/TASC.2022.3178359

Flux Pumping of Multiple Double-Loop Superconducting Structures for a Planar Magnetic Field Source

John H. Lacy, April Cridland, Jonathan Pinder, Alberto Uribe, Ryan Willetts, and José Verdú

***Abstract*— We discuss how flux pumping can be applied to multiple inductively coupled superconducting circuits, and describe its importance to the operation of a novel, planar magnetic field source for quantum technology applications. Specifically, we discuss how applying a transformer-rectifier flux pumping technique to several double-loop superconducting structures simultaneously allows for the effect of cross-talk — the inevitable coupling between neighbouring superconducting loops — to be accounted for. Using both a theoretical model and an experimental verification, we introduce a method of calibrating a flux-pumped magnetic field source such that any desired magnetic field distribution within the critical current limits of the used materials can be obtained.**

***Index terms*— Flux Pumping, Ion Traps, Quantum Technology, Superconducting Magnets.**

I. INTRODUCTION

Over the past two decades, there has been a significant shift towards the miniaturisation of quantum experiments and technologies. Such miniaturisation has many advantages and applications, including the improved scalability of ion-trap quantum computers [1]–[3], the development of atom chips for quantum sensing with condensates [4]–[6], and (more recently) towards tests of quantum gravity using Stern-Gerlach interferometry with chip-based traps [7]. The primary motivation for the work discussed herein is towards the miniaturisation of a planar magnetic field source for trapped electrons in a Penning trap [8]–[11] — the so-called *Geonium Chip* — which forms the functional hardware of a reliable and tunable single microwave photon detector [12], with potential applications in defense, microscopy, and communications [13]–[14]. Conventional Penning trap experiments use large, superconducting solenoids as their magnetic field source [15]-[16], similar to those used in Nuclear Magnetic Resonance (NMR) spectroscopy. To our knowledge, while remote magnetisation schemes have been successfully implemented in shim coils for NMR [17], flux pumping as a method for magnetisation or field shimming in an ion trap has never previously been employed. The magnetisation technique discussed here could also be useful for other scalable atomic experiments and quantum hardware, particularly chip-based traps for cold atoms and condensates.

Manuscript received February 24, 2022; revised April 28, 2022; accepted May 17, 2022.

This work was supported by EPSRC through grant no. EP/N00567.

J.H. Lacy is with Williams College, Williamstown, MA 01267, USA. (email: jhl4@williams.edu).

A. Cridland is with Swansea University, Singleton Campus, Swansea, SA2 8PP, UK.

J. Pinder, A. Uribe, R. Willetts, and J. Verdú are with the Geonium Chip Group, School of Mathematical & Physical Sciences, University of Sussex, Falmer BN1 9QH, UK.

In such experiments, high magnetic field stability and precise control of the magnetic field distribution are essential to their operation, yet the overall required magnetic field strengths are considerably lower than those required for a Penning trap (on the order of mT, rather than T [18]).

The Geonium Chip comprises a set of five DC electrodes which, when held at carefully chosen voltages, provide a trapping potential minimum at a height y_0 above the chip surface (see Figure 1a). Full confinement of an electron is achieved by applying a strong (> 0.1 T), homogeneous ($\partial_y B_z < 1\mathrm{mT\,mm^{-1}}$) magnetic field parallel to the chip surface, which is enclosed inside a cryogenic vacuum chamber at ~ 4 K. In its current formation (Figure 1b), this magnetic field source is provided by a set of planar current-driven loops of superconducting NbTi wire. The magnetic field lines from each loop add to produce a strong trapping field pointing parallel to the chip surface. This first-generation planar magnetic field source has been demonstrated to achieve a homogeneous trapping field of over 0.5 T [19]. A new magnetic field source is shown in Figure 1c. This is fabricated with closed superconducting loops that carry persistent currents, instead of driven currents as in [19]. This allows for much higher magnetic field stability, due to the elimination of both short-term fluctuations (less than one second) and long-term drifts (more than one second) that inevitably arise from current sources [20]. Furthermore, the closed superconducting loops (see Figure 1c) are progressively magnetised by the method of flux pumping [21]. This will allow for strong fields (0.1–1 T) to be generated with modest current sources (< 5 A), thus avoiding bulky high current vacuum feedthroughs. The ability to generate strong fields with such small flux pumping currents reduces the heat load in the cryostat, simplifying its design and operation.

The confinement and detection of a single electron requires extremely precise control of the magnetic field distribution [9]. As mentioned above, the overall magnetic field distribution is the superposition of the fields arising from each closed superconducting loop. If the currents are chosen carefully, the magnetic contributions from each loop add to produce a desired magnetic field distribution at one location, y_0. For the Geonium Chip, there may be more than one desired magnetic field distribution. For example, while a precise measurement of a trapped electron's motional frequencies relies on a highly homogeneous magnetic field (to first order, $\frac{\partial B_z}{\partial y} < 0.1 - 1.0\ \mathrm{mT\,mm^{-1}}$), single microwave photon detection, on the other hand, requires an inhomogeneous "magnetic bottle" field distribution: $\vec{B} = B_0\hat{z} + (B_2 \neq 0)z^2\hat{z}$, where $\hat{z}$ is the axial direction of the Penning trap (see

This article has been accepted for publication in IEEE Transactions on Applied Superconductivity. This is the author's version which has not been fully edited and content may change prior to final publication. Citation information: DOI 10.1109/TASC.2022.3178359

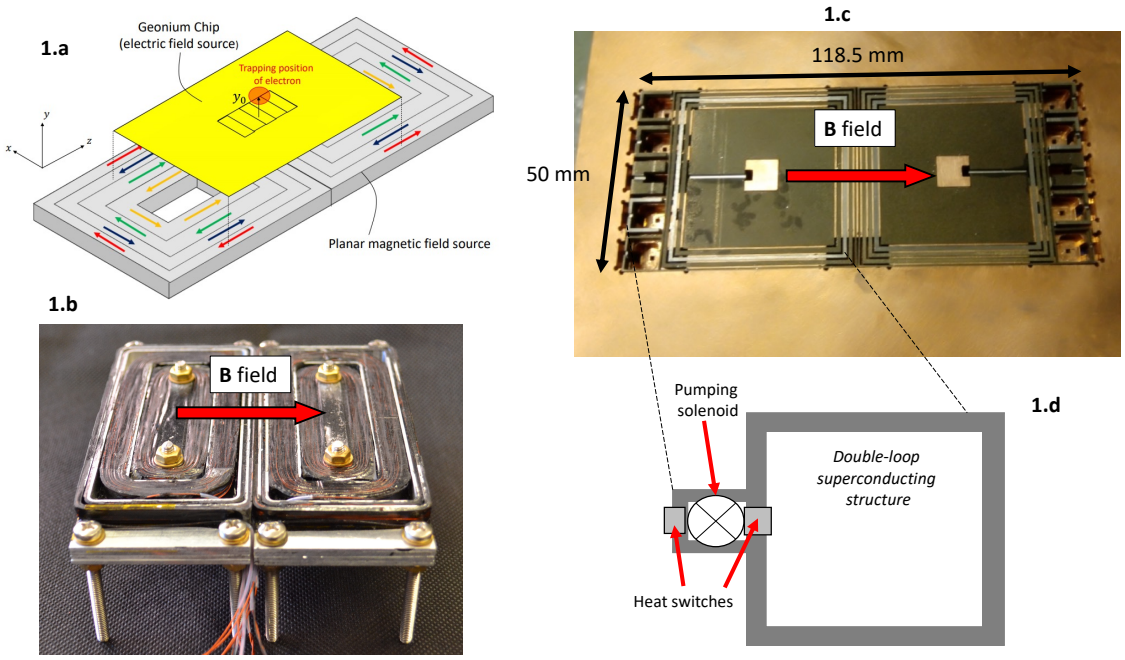

Fig. 1: **1a.** Schematic depiction of the Geonium Chip Penning Trap. The electric field source (yellow) is placed on top of a superconducting planar magnetic field source comprising several current-carrying closed loops of current. Electrons can be trapped a distance y_0 above the electric field source. **1b.** First generation planar magnetic field source for the Geonium Chip Penning Trap. This is made up of four pairs of NbTi coils carrying driven currents from high-precision power supplies. **1c.** Second generation superconducting planar magnetic field source for the Geonium Chip, comprising five pairs of double-loop superconducting structures. This field source is magnetised by a process of magnetic flux pumping, described in [21]. The effect of cross-talk between adjacent and overlapping coils is discussed in this paper. **1d.** A sketch of a double-loop superconducting structure, showing the location of heat switches and the pumping solenoid. Several of these make up the planar magnetic field source.

Figure 1a). This magnetic bottle allows for the detection of individual microwave photons through the continuous Stern-Gerlach effect [22]. Furthermore, in order for the Geonium Chip to act as a tunable microwave photon detector, control over the strength of the magnetic field (i.e., the B_0 term) is required. This is because the photon frequency detected by the electron, f_p, is directly proportional to the magnetic field strength, B_0, according to: $f_p \approx eB_0/2\pi m_e$, where e is the electron charge, and m_e is the electron mass. It is therefore vital that the Geonium Chip can precisely change the currents of the magnetic field source while the trap is operating, such that it can quickly (i.e., in a few seconds) go between different desired magnetic field distributions and strengths when required.

In the Geonium Chip, changes to the persistent currents of the magnetic field source need to be controlled with a fractional uncertainty of at most 10^{-5}. Precisely controlling more than one of these persistent currents is a challenge because of the well-known issue of flux conservation [23]. As is discussed extensively in the literature, when attempting to magnetise a closed superconducting loop, any change in applied magnetic flux through the closed superconducting contour is counteracted by the sudden induction of persistent current in that loop. This is often expressed algebraically as

$$\phi_{\mathrm{tot}} = \phi_{\mathrm{a}} + LI = \text{constant}, \tag{1}$$

where ϕ_{tot} is the total flux through a closed superconducting contour, and ϕ_{a} is the applied flux. LI represents the self-flux of the closed superconducting contour, where L is the self-inductance, and I is the current circulating in the loop. In actuality, there is an additional term $\oint_C \mu_0 \lambda^2 \mathbf{J} \cdot \mathrm{d}\mathbf{l}$ that describes the integral of the current density $\mathbf{J}$ along the closed superconducting contour C, where λ is the London penetration length. This term is negligible for the dimensions described herein (see [26]).

The well-established method of magnetic flux pumping allows for the magnetisation of a single closed superconducting loop by 'smuggling' small quantities of magnetic flux into a closed contour such that current is gradually built up over several cycles [24]. A recent summary of different methods of flux pumping can be found in [25]. As discussed in [21], the Geonium Chip makes use of a flux pumping scheme that uses a double-loop superconducting structure with two superconducting switches and a small pumping solenoid to build up hundreds of amperes, (see Figure 1d). However, in [21] the magnetic flux pumping of only one single superconducting loop is discussed. The magnetic field

This article has been accepted for publication in IEEE Transactions on Applied Superconductivity. This is the author's version which has not been fully edited and content may change prior to final publication. Citation information: DOI 10.1109/TASC.2022.3178359

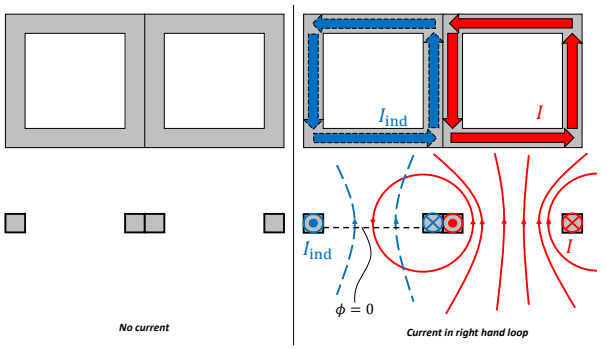

Fig. 2: A sketch of how cross-talk arises. **Left:** Two adjacently placed superconducting loops carrying no current. The top image is a top view, while the lower image gives a cross-sectional view. **Right:** The same loop configuration, but with current flowing in the right-hand loop. The magnetic field from the right-hand loop links into the left-hand loop. To ensure flux conservation, an induced current, I_{ind} flows in the left-hand loop to oppose the flux from the current in the right-hand loop.

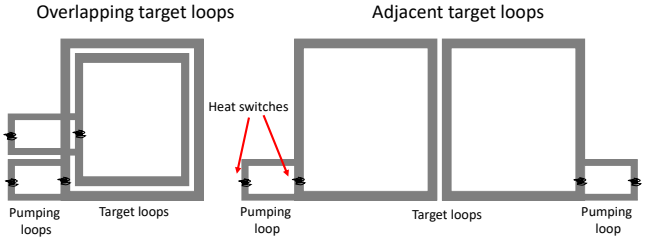

Fig. 3: A sketch showing the two different double-loop arrangements: **Left:** overlapping target loops, and **Right:** adjacent target loops. Locations of the heat switches are depicted for clarity.

for the Geonium Chip requires flux pumping of several superconducting loops (see Figure 1c). The difficulty here is that any time flux is changed in one of these double-loop superconducting structures, the resulting magnetic field from this loop also changes and leaks into neighbouring loops. The currents in these other loops (and their associated magnetic fields) consequently change, and one loses track and control of the overall magnetic field distribution. This "cross-talk" between loops is illustrated with a sketch of two superconducting loops in Figure 2. In order to overcome such cross-talk, precise control of the currents in each and every loop at any given time is needed.

This article discusses a scheme in which several of these double-loop superconducting structures are magnetised via flux pumping such that the currents in each loop can be well-controlled in spite of the occurrence of cross-talk. The crucial point is that the flux pumping steps described in [21] for one superconducting circuit are applied to each and every double-loop superconducting structure *simultaneously*. We demonstrate that while cross-talk is not eliminated, it is nevertheless accounted for in the sense that a linear mapping between the input fluxes, $\underline{\Phi}$, and the resulting overall magnetic field distribution, $\underline{B}$, exists. This is characterised by a calibration matrix, $\underline{\underline{\Theta}}$, which allows for any desired magnetic field distribution at y_0 to be achieved (so long as the critical current of the material is not exceeded). In section II, an analytical model is discussed which shows how this linear relationship arises for both adjacent and overlapping target loop arrangements. An experimental verification of the adjacent case is presented in section III, and a summary of the findings along with a discussion of future work is given in section IV.

II. SIMULTANEOUS FLUX PUMPING OF DOUBLE-LOOP SUPERCONDUCTING STRUCTURES

The persistent current planar magnetic field source in Figure 1c has been constructed by cutting a NbTi block into five pairs of double-loop superconducting structures. Each loop has a thickness of 1.0 mm, and their widths are chosen such that they produce a homogeneous magnetic field distribution ($B_z = B_0\hat{z}$) at a height of 1.6 mm above the magnetic field source when all loops have the same current density, J, where $B_0 \propto J$. More detail on the design of this magnetic field source can be found in [20]. Of relevance here are how the different superconducting structures interact. As can be seen, some of the double-loop superconducting structures are arranged in "adjacent configuration" (i.e., the target loops of the superconducting structures are laid side-by-side), and some are placed in "overlapping configuration" (i.e., with the target loops of the superconducting structures coaxially arranged) — see Figure 3. In this section, the effect of cross-talk in the two different configurations is discussed.

In order to have control over the final magnetic field distribution, it is necessary to flux pump the planar magnetic field source so that the final currents of each and every double-loop superconducting structure are linearly related to the set of input fluxes, which are controlled by the user. In its general mathematical form, this is expressed as

$$I_j = \sum_k K_{jk}\Phi_k, \tag{2}$$

where I_j is the final current in the jth double-loop structure, Φ_k is the input flux applied to the pumping loop of the kth double-loop structure, and K_{jk} is the matrix element that relates the two. For two non-interacting loops (1 and 2), each magnetised by input fluxes (ϕ_1 and ϕ_2), the final currents are given by

$$\begin{pmatrix} I_1 \\ I_2 \end{pmatrix} = \begin{pmatrix} K_{11} & 0 \\ 0 & K_{22} \end{pmatrix} \cdot \begin{pmatrix} \phi_1 \\ \phi_2 \end{pmatrix}. \tag{3}$$

For inductively coupled loops, the off-diagonal elements of K_{jk} ($j \neq k$) are non-zero, and describe the effect of cross-talk between the jth and kth superconducting structures.

Equation (2) describes how the currents resulting from flux pumping relate to the input fluxes. About y_0, the total magnetic field distribution arising from these currents,

This article has been accepted for publication in IEEE Transactions on Applied Superconductivity. This is the author's version which has not been fully edited and content may change prior to final publication. Citation information: DOI 10.1109/TASC.2022.3178359

$\underline{B} = (B_z, \partial_y B_z, \partial^2_{y^2} B_z, ...)$ is the sum of magnetic field contributions from each current $\underline{I} = (I_1, I_2, I_3, ...)$. This relationship can be represented as a matrix,

$$\begin{pmatrix} B_z \\ \partial_y B_z \\ \vdots \\ \partial^n_{y^n} B_z \end{pmatrix} = \begin{pmatrix} \Gamma_{11} & \Gamma_{12} & \dots & \Gamma_{1n} \\ \Gamma_{21} & \Gamma_{22} & \dots & \Gamma_{2n} \\ \vdots & \vdots & \ddots & \vdots \\ \Gamma_{n1} & \Gamma_{n2} & \dots & \Gamma_{nn} \end{pmatrix} \cdot \begin{pmatrix} I_1 \\ I_2 \\ \vdots \\ I_n \end{pmatrix}. \quad (4)$$

or, in elemental form,

$$B_i = \sum_j \Gamma_{ij} I_j. \quad (5)$$

The elements of $\underline{\underline{\Gamma}}$ relate the currents in each loop to the spatial properties of the magnetic field. Substituting (2) into (5) gives us the desired linear relationship between the final magnetic field distribution and the input fluxes applied to each double-loop superconducting structure:

$$B_i = \sum_j \sum_k \Gamma_{ij} K_{jk} \Phi_k = \sum_k \Theta_{ik} \Phi_k. \quad (6)$$

Practically speaking, the set of input fluxes $\underline{\Phi}$ is provided by applying pumping currents, $\underline{I}^{(p)}$, to small pumping solenoids located in the pumping loops of the magnetic field source (see section III). Mathematically, these pumping currents, $\underline{I}^{(p)}$, are related to the applied fluxes by $\underline{\Phi} = \underline{\underline{L}} \cdot \underline{I}^{(p)}$, where $\underline{\underline{L}}$ is a diagonal matrix of the pumping solenoid inductances. Substituting into equation (6), this becomes

$$B_i = \sum_j \sum_k \Theta_{ij} L_{jk} I^{(p)}_k = \sum_k \chi_{ik} I^{(p)}_k. \quad (7)$$

While equation (7) is more practically useful (and is used in section III), the theoretical discussion presented here will be discussed in terms of fluxes, $\underline{\Phi}$, instead of pumping currents, $\underline{I}^{(p)}$.

In this section, we will apply the principles of flux conservation along with the linear flux approximation — the condition that, for thin current-carrying loops, the self-inductance of a loop is directly proportional to the loop's perimeter [21] — to demonstrate that the linear relationship of equation (6) is maintained for both the adjacent and overlapping cases, so long as all structures are flux pumped simultaneously. It should be noted that in the flux pumping schemes described below, the same assumptions as discussed in [21] are used.

A. Overlapping loop arrangement

Figure 4 shows the flux pumping scheme applied to two double-loop superconducting structures in the overlapping loop arrangement. The target and pumping loops of both superconducting structures are squares of length, l, and are assumed to be of dimensions such that the linear flux approximation [21] is valid. Under this approximation, the self-flux of a loop carrying a current, I, is given by: $LI = k \times$ "loop perimeter" $\times I$. The proportionality constant, k, will be used extensively throughout. The target loops of the upper (S1) and lower (S2) double-loop superconducting structures are assumed to carry initial currents of I_1 and I_2 respectively. Moreover, the fraction of flux from the target loop of one superconducting structure that couples to the other is given by m. Note that in Figure 4, the target loop of S2 is placed on top of the target loop of S1 (see the side view image in Figure 4). The simultaneous flux pumping mechanism can be summarised with the following steps:

- **Step 1**: *Turn ON the heating current to Heat Switch 1 of BOTH double-loop structures simultaneously to locally break the superconductivity, so as to OPEN the switches.*
  There are two relevant superconducting contours, corresponding to the two overlapping target loops. There is no change in current in either loop.
- **Step 2:** *Turn ON the input currents to the pumping solenoids of S1 and S2 to provide input fluxes of ϕ_1 and ϕ_2 respectively.*
  Assuming no stray flux lines from the solenoids link into any of the target loops, there is no change in current in either superconducting structure.
- **Step 3:** *Turn OFF the heating current to Heat Switch 1 of both superconducting structures to restore the superconductivity.*
  Here, there is no change in current in either superconducting structure.
- **Step 4:** *Turn ON the heating current to Heat Switch 2 of both superconducting structures so as to OPEN the two switches simultaneously.*
  The currents are now redistributed to the outer loops of each respective superconducting structure, and their values are transformed according to $\{I_1, I_2\} \rightarrow \{I'_1, I'_2\}$. A detailed depiction of this step is given in Figure 5, where the overlapping target loops are shown separated for the sake of clarity. Consider the total flux through the contour defining the perimeter of S1, represented by the dashed blue line. Before step 4 is implemented, the total flux through this contour is the sum of the applied flux, ϕ_1, the self-flux, $3klI_1$ (note, there is no net flux contribution from the current along the bridge joining the pumping and target loops), and the cross-talk from S2, $3klI_2m$. After the step, the total flux in S2 is now given by the sum of the applied flux, ϕ_1, the self-flux, $6klI'_1$, and the cross-talk from S2, $2klI'_2m$. Similar expressions can be written down for S2. Due to flux conservation, the following equations must be satisfied:

Upper double–loop structure (S1)

$$3klI_1 + 3klI_2m + \phi_1 = 6klI'_1 + 2klI'_2m + \phi_1, \quad (8)$$

Lower double–loop structure (S2)

$$3klI_1m + 3klI_2 + \phi_2 = 6klI'_2 + 2klI'_1m + \phi_2, \quad (9)$$

where the left-hand side of each equation describes the flux before step 4, and the right-hand side describes the

This article has been accepted for publication in IEEE Transactions on Applied Superconductivity. This is the author's version which has not been fully edited and content may change prior to final publication. Citation information: DOI 10.1109/TASC.2022.3178359

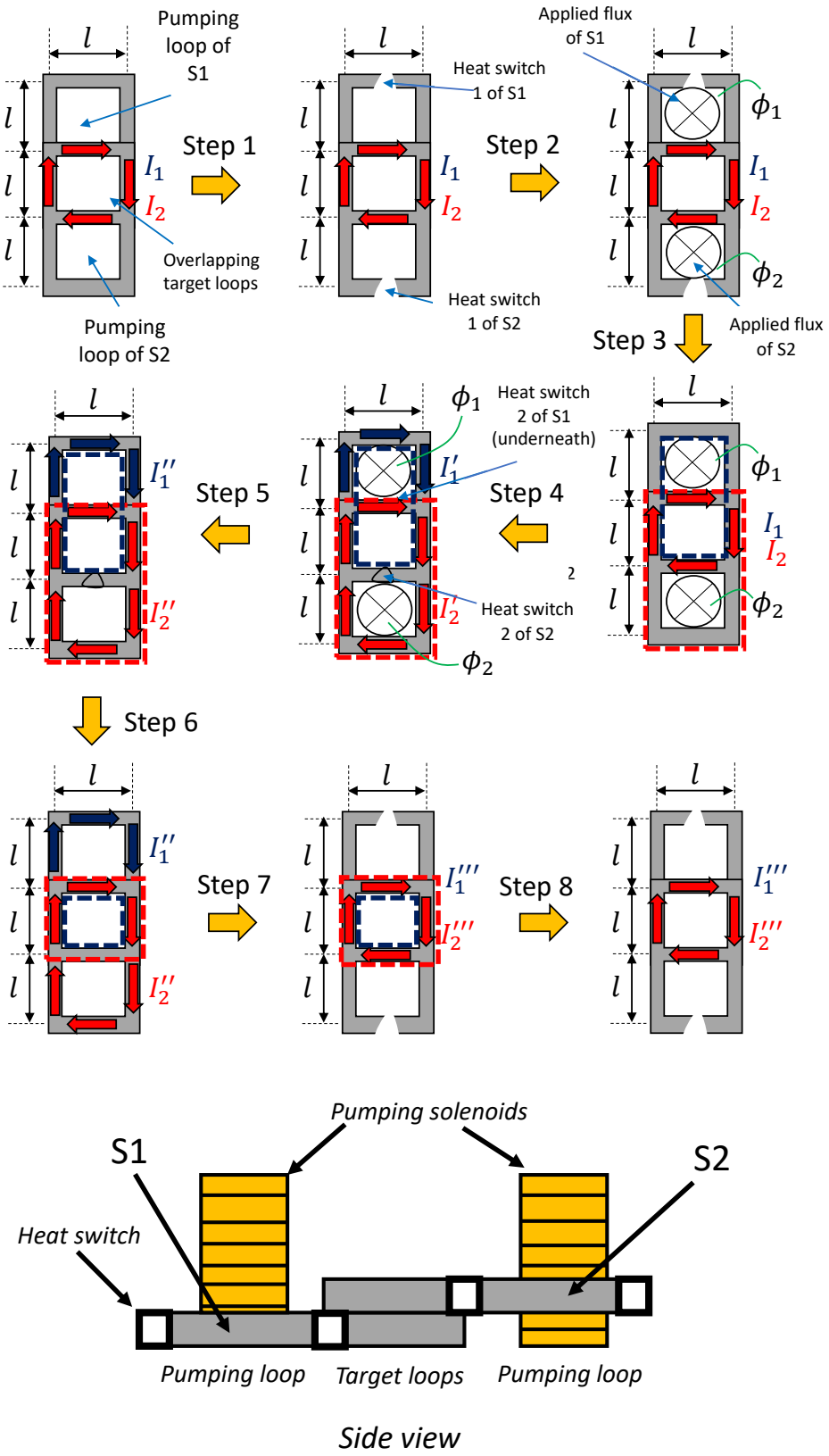

Fig. 4: Flux pumping scheme of two double-loop superconducting structures with overlapping target loops. The target loop of S2 is placed on top of the target loop of S1. Current in S1 is represented by a blue arrow. Current in S2 is depicted by a red arrow. Applied flux is represented by ⊗, which indicates that the magnetic field lines are pointing into the page.

This article has been accepted for publication in IEEE Transactions on Applied Superconductivity. This is the author's version which has not been fully edited and content may change prior to final publication. Citation information: DOI 10.1109/TASC.2022.3178359

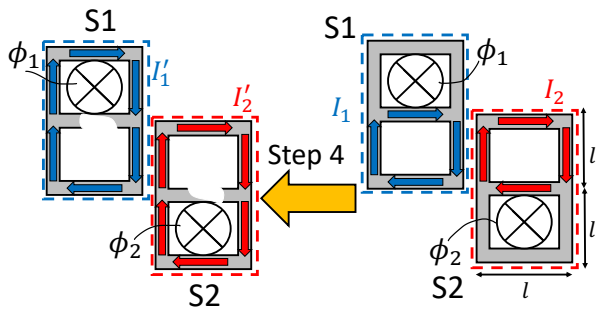

Fig. 5: Detailed depiction of step 4 from the flux pumping scheme of Figure 4. The target loops are separated here for visual purposes.

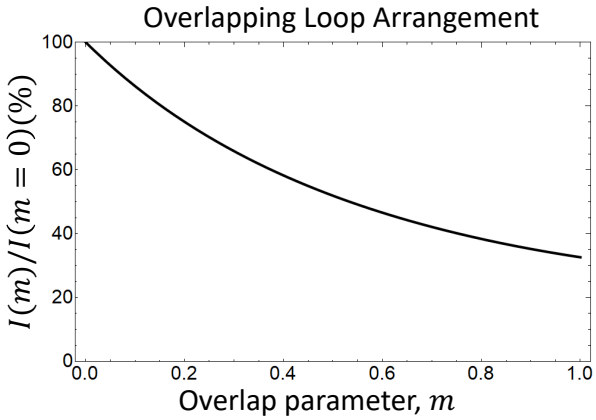

Fig. 6: Graph showing the flux pump efficiency for the overlapping loop arrangement as a function of overlap parameter, m. The curve shows the efficiency when the input fluxes have the same polarity and magnitude ($\Phi = (\phi, \phi)$).

flux after the step. Representing equations (8) and (9) in vector-matrix form, gives

$$\begin{pmatrix} I_1' \\ I_2' \end{pmatrix} = \frac{1}{36-4m^2} \begin{pmatrix} 18-6m^2 & 12m \\ 12m & 18-6m^2 \end{pmatrix} \cdot \begin{pmatrix} I_1 \\ I_2 \end{pmatrix}. \tag{10}$$

- **Step 5:** *Turn OFF the input currents to the solenoids so as to remove the applied fluxes, ϕ_1 and ϕ_2.*
  Removing ϕ_1 and ϕ_2 results in a jump in current in both superconducting structures such that $\{I_1', I_2'\} \rightarrow \{I_1'', I_2''\}$. Following the same reasoning for step 4 gives:

Upper double–loop structure (S1)

$$6klI_1' + 2klI_2'm + \phi_1 = 6klI_1'' + 2klI_2''m. \tag{11}$$

Lower double–loop structure (S2)

$$6klI_2' + 2klI_1'm + \phi_2 = 6klI_2'' + 2klI_1''m. \tag{12}$$

In vector-matrix form, these are represented as

$$kl \begin{pmatrix} 6 & 2m \\ 2m & 6 \end{pmatrix} \cdot \begin{pmatrix} I_1' \\ I_2' \end{pmatrix} + \begin{pmatrix} \phi_1 \\ \phi_2 \end{pmatrix} = kl \begin{pmatrix} 6 & 2m \\ 2m & 6 \end{pmatrix} \cdot \begin{pmatrix} I_1'' \\ I_2'' \end{pmatrix}. \tag{13}$$

Solving for $\underline{I}'' = (I_1'', I_2'')$, we get

$$\begin{pmatrix} I_1'' \\ I_2'' \end{pmatrix} = \frac{1}{36-4m^2} \begin{pmatrix} 18-6m^2 & 12m \\ 12m & 18-6m^2 \end{pmatrix} \cdot \begin{pmatrix} I_1 \\ I_2 \end{pmatrix} + \frac{1}{kl\,(36-4m^2)} \begin{pmatrix} 6 & -2m \\ -2m & 6 \end{pmatrix} \cdot \begin{pmatrix} \phi_1 \\ \phi_2 \end{pmatrix}. \tag{14}$$

- **Step 6:** *Turn OFF the heating currents to Heat Switch 2 of each double-loop structure so as to CLOSE the switches.*
  There are no current changes in this step.
- **Step 7:** *Turn ON the heating currents to Heat Switch 1 of each superconducting structure so as to OPEN the switches.*
  Here, the current is redirected to the target loop of each superconducting structure. The currents are transformed according to $\{I_1'', I_2''\} \rightarrow \{I_1''', I_2'''\}$. Applying flux conservation, the currents become

Upper double–loop structure (S1)

$$3klI_1'' + 3klI_2''m = 4klI_1''' + 4klI_2'''m. \tag{15}$$

Lower double–loop structure (S2)

$$3klI_1''m + 3klI_2'' = 4klI_1''m + 4klI_2'''. \tag{16}$$

The equations above, represented in vector-matrix form, are given as follows:

$$\begin{pmatrix} I_1''' \\ I_2''' \end{pmatrix} = \frac{(12-12m)}{(16-16m^2)\,(36-4m^2)} \times \left[\begin{pmatrix} (18-6m^2) & 12m \\ 12m & (18-6m^2) \end{pmatrix} \cdot \begin{pmatrix} I_1 \\ I_2 \end{pmatrix} + \frac{1}{kl} \begin{pmatrix} 6 & -2m \\ -2m & 6 \end{pmatrix} \cdot \begin{pmatrix} \phi_1 \\ \phi_2 \end{pmatrix} \right]. \tag{17}$$

- **Step 8:** *Turn OFF the heating currents to Heat Switch 1 of each superconducting structure so as to CLOSE the switches.* There are no current changes in this step.

The current vector, $\underline{I}''' = (I_1''', I_2''')$, describes the final current after one flux pumping cycle in terms of the initial current, $\underline{I} = (I_1, I_2)$, and the input fluxes, $\underline{\Phi} = (\phi_1, \phi_2)$. This equation can be written, without loss of generality, as the current vector, $\underline{I}_n = (I_n^{(1)}, I_n^{(2)})$ after n cycles, in terms of the current after $n-1$ cycles, $\underline{I}_{n-1} = (I_{n-1}^{(1)}, I_{n-1}^{(2)})$:

This article has been accepted for publication in IEEE Transactions on Applied Superconductivity. This is the author's version which has not been fully edited and content may change prior to final publication. Citation information: DOI 10.1109/TASC.2022.3178359

$$\begin{pmatrix} I_n^{(1)} \\ I_n^{(2)} \end{pmatrix} = \frac{(12-12m)}{(16-16m^2)\,(36-4m^2)} \times \left[\begin{pmatrix} (18-6m^2) & 12m \\ 12m & (18-6m^2) \end{pmatrix} \cdot \begin{pmatrix} I_{n-1}^{(1)} \\ I_{n-1}^{(2)} \end{pmatrix} + \frac{1}{kl} \begin{pmatrix} 6 & -2m \\ -2m & 6 \end{pmatrix} \cdot \begin{pmatrix} \phi_1 \\ \phi_2 \end{pmatrix} \right], \tag{18}$$

In general form, this is rendered as:

$$\underline{I}_n = \underline{\underline{U}} \cdot \underline{I}_{n-1} + \underline{\underline{V}} \cdot \underline{\Phi}. \tag{19}$$

If $n = N$, the vector describing the current in each loop becomes

$$\underline{I}_N = (\underline{\underline{1}} - \underline{\underline{U}})^{-1} \cdot (\underline{\underline{1}} - \underline{\underline{U}}^N) \cdot \underline{\underline{V}} \cdot \underline{\Phi}. \tag{20}$$

Despite the apparent complexity of equation (20), it has the important feature that the magnetic field distribution is linearly related to the input fluxes, as desired. Note that for a large number of flux pumping cycles (i.e., $N \to \infty$), the final current configuration becomes

$$\lim_{N\to\infty} \underline{I}_N = \left(\underline{\underline{1}} - \underline{\underline{U}}\right)^{-1} \cdot \underline{\underline{V}} \cdot \underline{\Phi}, \tag{21}$$

where it is noted that $\det \underline{\underline{U}} < 1$. Relating the currents to the overall magnetic field distribution (equation (5)), we see that

$$\underline{B} = \underline{\underline{\Gamma}} \cdot \left(\underline{\underline{1}} - \underline{\underline{U}}\right)^{-1} \cdot \underline{\underline{V}} \cdot \underline{\Phi} \equiv \underline{\underline{\Theta}} \cdot \underline{\Phi}. \tag{22}$$

The presence of cross-talk therefore does not change the linear relationship between the input fluxes, $\underline{\Phi}$, and the overall magnetic field distribution, $\underline{B}$. Thus, so long as each loop is flux pumped simultaneously, any arbitrary current configuration (and, consequently, magnetic field distribution) can be achieved if the correct input fluxes are applied to each structure.

Before flux pumping of the adjacent loop arrangement is discussed, it is worth exploring how the final obtainable currents are affected by the degree of coupling (or "overlap parameter"), m, of the two target loops, which can take any value in the range $0 \leq m \leq 1$. The extreme case of $m = 0$ refers to the loops being completely separate, such that there is no cross-talk between them. Assuming input fluxes $\phi_1 = \phi_2 = \phi$, the final currents are the same as when calculated individually (i.e., each loop carrying $I(m = 0) = \phi/5kl$ of current). The other extreme, when $m = 1$, refers to the case when the target loops of both superconducting structures perfectly overlap. Once again, if we assume $\phi_1 = \phi_2 = \phi$, then the final current in each loop becomes $I(m = 1) = 3\phi/46kl$. Thus, the presence of cross-talk between perfectly overlapping target loops reduces the efficiency to $3/46 \div 1/5 \approx 32.6\%$ compared with the case where there is no cross-talk. The relationship between final obtainable currents and m is shown in Figure 6. It is important to point out that, while there is a significant reduction in efficiency, simultaneous flux pumping still allows for current build up in both loops even in the case of perfect target loop overlap ($m = 1$). This means that even the inner overlapping loops of the magnetic field source in Figure 1c will be magnetised despite their target loops being located entirely within the target loops of the outer superconducting structures.

B. Adjacent loop arrangement

Now consider the two double-loop structures placed in an adjacent arrangement, as shown in Figure 7. Here the target loop of the left-hand structure carries a clockwise circulating initial current, I_1, and the target loop of the right-hand structure carries a clockwise initial current of I_2. The flux pumping scheme here has exactly the same steps as for the case with overlapping target loops, and so will not be repeated in unnecessary detail. Here, m describes the fraction of flux that couples from the left-hand target loop into the right-hand target loop (and *vice versa*) from the current in the edges of the target loops that are touching. As can be seen in Figure 7, current changes only occur in steps 4, 5, and 7. Using the same reasoning as before, the currents, $\underline{I}' = (I_1', I_2')$, after step 4 satisfy the following equations:

Left–hand double loop

$$3klI_1 + \phi_1 - klI_2m = 6klI_1' + \phi_1 - klI_2'm, \tag{23}$$

Right–hand double loop

$$3klI_2 + \phi_2 - klI_1m = 6klI_2' + \phi_2 - klI_1'm. \tag{24}$$

Solving for $\underline{\underline{I}}'$, we obtain:

$$\begin{pmatrix} I_1' \\ I_2' \end{pmatrix} = \frac{1}{36-m^2} \begin{pmatrix} 18-m^2 & -3m \\ -3m & 18-m^2 \end{pmatrix} \cdot \begin{pmatrix} I_1 \\ I_2 \end{pmatrix}. \tag{25}$$

The next step where there is a change in current is step 5, where the current transformation $\{I_1', I_2'\} \to \{I_1'', I_2''\}$ occurs. Applying flux conservation to the outer loop of each superconducting structure gives

Left–hand double loop

$$6klI_1'' + \phi_1 - klI_2'm = 6klI_1'' - klI_2''m, \tag{26}$$

Right–hand double loop

$$6klI_2' + \phi_2 - klI_1'm = 6klI_2'' - klI_1''m, \tag{27}$$

which can be reformed as

$$\begin{pmatrix} I_1'' \\ I_2'' \end{pmatrix} = \begin{pmatrix} I_1' \\ I_2' \end{pmatrix} + \frac{1}{(36-m^2)\,kl} \begin{pmatrix} 6 & m \\ m & 6 \end{pmatrix} \cdot \begin{pmatrix} \phi_1 \\ \phi_2 \end{pmatrix},$$
$$\Rightarrow \begin{pmatrix} I_1'' \\ I_2'' \end{pmatrix} = \frac{1}{36-m^2} \left[\begin{pmatrix} 18-m^2 & -3m \\ -3m & 18-m^2 \end{pmatrix} \cdot \begin{pmatrix} I_1 \\ I_2 \end{pmatrix} + \frac{1}{kl} \begin{pmatrix} 6 & m \\ m & 6 \end{pmatrix} \cdot \begin{pmatrix} \phi_1 \\ \phi_2 \end{pmatrix} \right]. \tag{28}$$

This article has been accepted for publication in IEEE Transactions on Applied Superconductivity. This is the author's version which has not been fully edited and content may change prior to final publication. Citation information: DOI 10.1109/TASC.2022.3178359

The final current change comes in step 7. Applying flux conservation in the target loops of each double-loop structure, the final current after one flux pumping cycle is given by

$$\begin{pmatrix} I_1''' \\ I_2''' \end{pmatrix} = \frac{1}{(16-m^2)(36-m^2)} \begin{pmatrix} 12-m^2 & -m \\ -m & 12-m^2 \end{pmatrix} \cdot \left[\begin{pmatrix} 18-m^2 & -3m \\ -3m & 18-m^2 \end{pmatrix} \begin{pmatrix} I_1 \\ I_2 \end{pmatrix} + \frac{1}{kl} \begin{pmatrix} 6 & m \\ m & 6 \end{pmatrix} \begin{pmatrix} \phi_1 \\ \phi_2 \end{pmatrix} \right]. \tag{29}$$

Once again, we argue that, without loss of generality, equation (29) can be rewritten as

$$\underline{I}_n = \underline{\underline{U'}}.\underline{I}_{n-1} + \underline{\underline{V'}}.\underline{\Phi}, \tag{30}$$

thereby demonstrating the linearity of the flux pumping scheme. Using a similar expression to equation (21), the final currents after a large number of cycles can be calculated. In the limiting case of no coupling between adjacent loops (i.e., $m = 0$), the final currents, as expected, are the same as when calculated individually (i.e., $I = \phi/5kl$). In the extreme case of maximum coupling, (i.e., $m = 1$), the final current is $I(m = 1)/I(m = 0) = 2/11 \div 1/5 \approx 90.9\%$. Interestingly, with an applied flux of $\Phi = (\phi, -\phi)$, the final current for $m = 1$ exceeds the case for $m = 0$: $I(m = 1)/I(m = 0) = 4/19 \times 5 \approx 105.3\%$. The extra degree of efficiency comes from the fact that with opposite input fluxes, the currents on the touching edges of the target loops are now pointing in the same direction. The efficiency as a function of overlap parameter, m, is shown in Figure 8 for both cases.

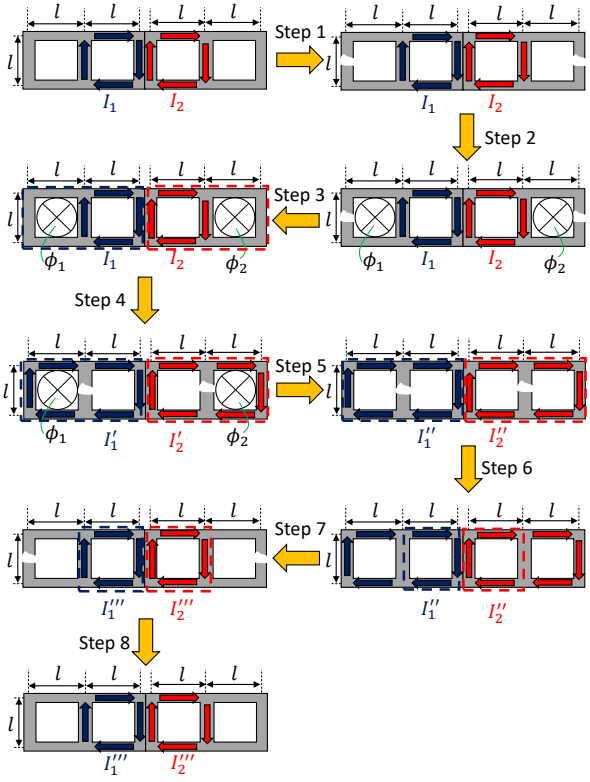

Fig. 7: Flux pumping scheme of two double-loop superconducting structures with adjacently placed target loops. Current in the left-hand double-loop structure is represented by blue arrows, while current in the right-hand superconducting double-loop structure is depicted by red arrows. Applied flux is represented by ⊗.

III. Experimental Verification

Section II showed that, despite the presence of cross-talk, simultaneous flux pumping of multiple double-loop superconducting structures results in a linear relationship between the input fluxes and the final magnetic field distribution. In this section, an experimental verification of this linear relationship in the case of adjacently placed target loops is presented. While not experimentally investigated here, we argue that this linear relationship will also apply to the case of overlapping target loops, since such a difference will manifest only in different values of the matrix elements of Θ (or χ), and not in the overall mathematical form of the relationship. Furthermore, this should also extend to any arbitrary number of double-loop superconducting structures. For n independent double-loop superconducting structures, the resulting calibration matrix, Θ (or χ), will have dimension $n \times n$.

A. Experimental setup

An illustration of the experimental setup is given in Figure 9. Two double-loop superconducting structures were

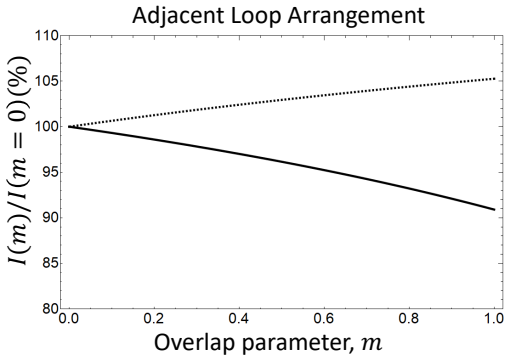

Fig. 8: Graph showing the flux pump efficiency for the adjacent loop arrangement as a function of overlap parameter, m. The solid curve shows the efficiency when the input fluxes have the same polarity. The dashed curve shows the efficiency with input fluxes with opposite polarity.

This article has been accepted for publication in IEEE Transactions on Applied Superconductivity. This is the author's version which has not been fully edited and content may change prior to final publication. Citation information: DOI 10.1109/TASC.2022.3178359

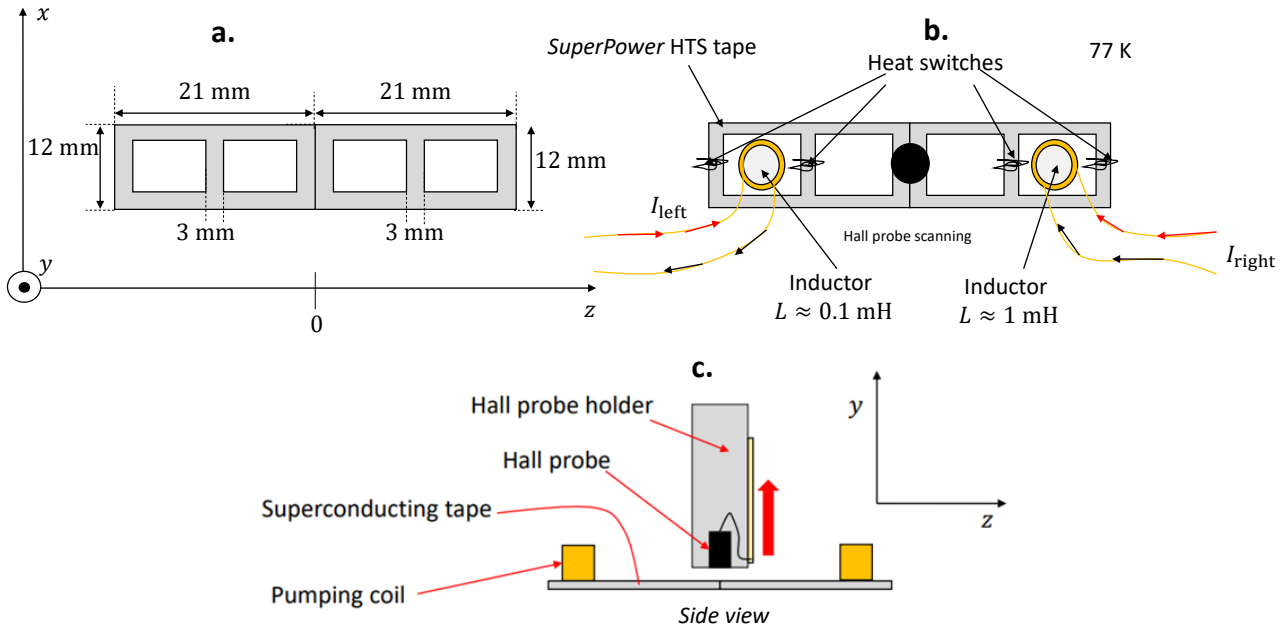

Fig. 9: Schematic of the experimental setup to measure the cross-talk between two adjacently separated double-loop superconducting structures. **a.** Top view showing the dimensions of the two double-loop superconducting structures made from *SuperPower* HTS tape. **b.** Top view of the experimental setup, showing the locations of the heat switches, the pumping solenoids, and the position of the Hall Probe. **c.** Side view of the experimental setup, showing the direction over which the Hall probe was scanned.

cut from a strip of 12 mm unstabilised high temperature superconductor (HTS) tape from *SuperPower Inc.* using a *Hei-Z* CNC milling machine. Both adjacent superconducting structures were cut to the same dimensions, with the pumping and target loops equal in size. Superconducting switches were placed on the central bridge and outer edge of each superconducting structure, and were made by wrapping several turns of nickel chromium wire (of resistance per unit length $\rho = 66\ \Omega\,\mathrm{m}^{-1}$) around the tape and coating with varnish to prevent heat loss via convection in the liquid nitrogen bath. To operate these heat switches, 1 A of current was supplied from a four-channel *HMP4040 Rohde & Schwarz* power supply. To ensure simultaneity of heat switch operation, both edge switches were connected in series to channel 1 of the power supply, and both bridge switches were connected in series to channel 2. In each pumping loop, small pumping solenoids were placed comprising many turns ($\sim$1000 turns for the left hand solenoid, $\sim$100 turns for the right hand solenoid) of 0.056 mm enamelled copper wire wrapped around a 3 mm screw. The cores of the left and right hand solenoids were made from brass and steel respectively. The inductances were $L_{\text{left}} \approx 0.1$ mH and $L_{\text{right}} \approx 1.0$ mH. The screw heads were placed face down in the respective pumping coils and were connected to channels 3 an 4 of the high precision *HMP4040 Rohde & Schwarz* power supply. The electrical setup was placed inside a polystyrene container holding 10 litres of liquid nitrogen located on the bed the *Hei-Z* CNC machine. An *Arepoc* cryogenic Hall probe was attached to the moving head of the CNC machine, so that the Hall probe position could be computer controlled with step resolution of 0.003 mm. The Hall probe was placed such that the active area was positioned to be at $r_0 = (x_0, y_0, z_0) = (0.00, 1.00, 0.00)$ mm in the coordinate system shown in Figure 9a.

B. Results and discussion

The first step was to calibrate the system by measuring the magnetic field distribution from the current configurations: $\underline{I} = (I_{\mathrm{L}}, I_{\mathrm{R}}) = (0.10, 0.00)$ A and $\underline{I} = (I_{\mathrm{L}}, I_{\mathrm{R}}) = (0.00, 0.10)$ A. I_L and I_R refer to the input currents to the solenoids of the left- and right-hand double-loop superconducting structures respectively. For each set of input currents, the system was flux pumped to saturation (see Figure 10), after which the Hall Probe was scanned a distance of ± 0.25 mm about r_0 in the y direction. Additionally, scans of the background magnetic field distribution were performed and subtracted from the flux pumped magnetic field distribution, to eliminate any effects due to stray fields (such as the Earth's magnetic field). After background subtraction, the resulting magnetic field distributions were then fit to a fourth order polynomial in $(y - y_0)$:

$$B_z(y) = B_{z0} + B_{z1}(y - y_0) + \cdots + B_{z4}(y - y_0)^4, \quad (31)$$

This article has been accepted for publication in IEEE Transactions on Applied Superconductivity. This is the author's version which has not been fully edited and content may change prior to final publication. Citation information: DOI 10.1109/TASC.2022.3178359

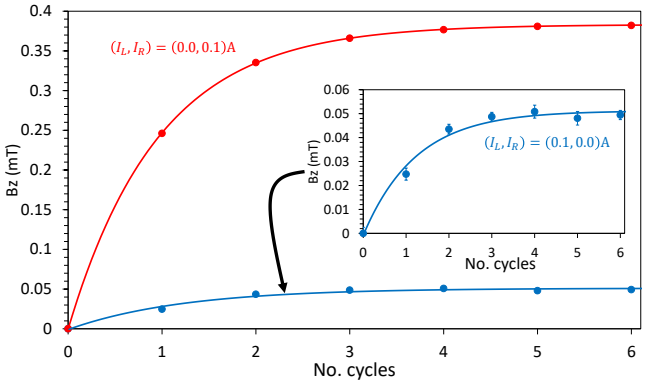

Fig. 10: Flux pumping calibration graphs showing $B_z(r_0)$ as a function of cycle number. Saturation is effectively reached after 5 flux pumping cycles. Due to the difference in solenoid inductances, the final magnetic field of the $\underline{I} = (0.00, 0.10)$ A case is a factor of 7.6 times larger than the final magnetic field achieved with a set of input currents given by $\underline{I} = (0.10, 0.00)$ A.

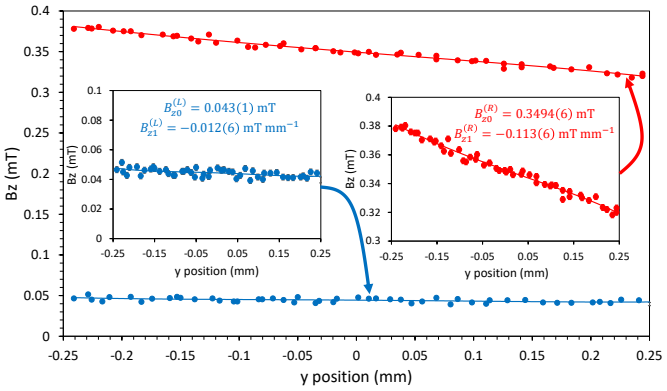

Fig. 11: Measured magnetic field distributions for the two calibration cases showing the zeroth and first order fit parameters.

where $B_{zi} = \frac{\partial^i B_z}{\partial y^i}\Big|y_0$. Results of two of these fits are given in Figure 10, where the zeroth and first order terms are displayed. These coefficients define the calibration of the setup, and can be summarised (per 1 A of input current) in matrix form as follows:

$$\underline{\underline{\chi}} = \begin{pmatrix} b_{z0}^{(L)} & b_{z0}^{(R)} \\ b_{z1}^{(L)} & b_{z1}^{(R)} \end{pmatrix}, \tag{32}$$

where $b_{zi}^{(L)} = B_{zi}^{(L)}/1\text{A}$ for the left-hand loop (L), with similar expressions for the right-hand loop (R). The results from the calibration measurement are summarised as

$$\underline{\underline{\chi}} = \begin{pmatrix} 0.43(1) & 3.494(6) \\ -0.12(6) & -1.13(6) \end{pmatrix} \begin{matrix} \text{mT A}^{-1} \\ \text{mT mm}^{-1} \end{matrix} \tag{33}$$

where the units for each row are displayed on the right.

Using the matrix elements given in (33), one can calculate the expected values of the magnetic field coefficients B_{z0}^{exp} and B_{z1}^{exp} for any arbitrary pair of applied currents. Two explicit cases are presented here, one with an even set of input currents $(I_{\text{left}}, I_{\text{right}}) = (0.31, 0.31)$ A and one with an odd set of currents $(I_{\text{left}}, I_{\text{right}}) = (0.31, -0.31)$ A. Using the same steps as described above, the two double-loop superconducting structures were flux pumped to saturation and the magnetic field distribution was measured by scanning the Hall probe about r_0. A comparison between the predicted coefficient values (using $\underline{\underline{\chi}}$ in equation (33)) and measured magnetic field distribution values is given in Table I. It shows that the measured and predicted magnetic field distributions agree within the quoted error bars, clearly demonstrating the validity and linearity of our calibration method.

$\underline{I}_a = (I_{\text{left}}, I_{\text{right}})$(A)	B_{z0}^{exp} (mT)	B_{z0}^{meas} (mT)
$(0.31, 0.31)$	$1.22(1)$	$1.21(1)$
$(0.31, -0.31)$	$-0.95(1)$	$-0.94(1)$

$\underline{I}_a = (I_{\text{left}}, I_{\text{right}})$(A)	B_{z1}^{exp}(mT mm^{-1})	B_{z1}^{meas}(mT mm^{-1})
$(0.31, 0.31)$	$-0.39(4)$	$-0.40(1)$
$(0.31, -0.31)$	$0.31(4)$	$0.29(2)$

TABLE I: Table comparing the expected and measured magnetic field distributions. The expected magnetic field distributions are calculated based on the magnetic field distributions from the calibration input currents of $\underline{I} = (0.1, 0.0)$ A and $\underline{I} = (0.0, 0.1)$ A.

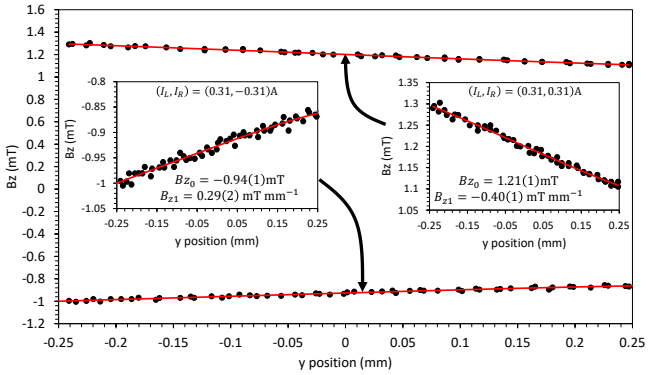

Fig. 12: A graph showing the magnetic field distributions for the two cases, with input fluxes $(I_L, I_R) = (0.31, 0.31)$ A and $(I_L, I_R) = (0.31, -0.31)$ A. The measured magnetic field distributions are in excellent agreement with the predicted values.

IV. CONCLUSIONS

In this article, we investigated how simultaneously flux pumping two inductively coupled double-loop superconducting structures affects the overall magnetic field distribution that is achieved. Using small superconducting circuits made from HTS tape, we fluxed pumped and measured the resulting magnetic field distribution from an adjacent arrangement of superconducting structures. In this simple system, we found that the overall magnetic field distribution and pumping currents (which are proportional to the input fluxes, $\underline{\Phi}$), are linearly related by a calibration matrix, $\underline{\underline{\chi}}$.

This means that, once $\underline{\underline{\chi}}$ is known, any desired magnetic field distribution, $\underline{B}_{\mathrm{des}}$, can be achieved by simply choosing the appropriate pumping currents, $\underline{I}_{\mathrm{req}}^{(p)}$. These are obtained from the following transformation:

$$\underline{I}_{\mathrm{req}}^{(p)} = \underline{\underline{\chi}}^{-1} \cdot \underline{B}_{\mathrm{des}}. \tag{34}$$

While only the case of adjacently arranged superconducting structures was experimentally investigated, our theoretical model suggests that a similar relationship should also be obtained in the overlapping arrangement. This will be investigated experimentally in future work.

Another obvious extension to the work discussed here is to investigate the simultaneous flux pumping of several (> 2) superconducting structures. While our model suggests that the same principles discussed above should also apply to any number of interacting double-loop superconducting structures, the added complexity of having many interacting loops presents several practical challenges. An important example is how with the overlap parameter, m, (which implicitly affects the matrix elements of $\underline{\underline{\Theta}}$ and $\underline{\underline{\chi}}$) will vary in complex, multi-loop systems. As shown in Figures 6 and 8, the final obtainable currents (and hence magnetic fields) from this flux pumping scheme is highly sensitive to this overlap parameter. For the new magnetic field source of the Geonium Chip shown in Figure 1c, which has five pairs of double-loop superconducting structures, how this will affect the maximum achievable field strength will have to be investigated empirically. A systematic characterisation of how m varies for different arrangements of double-loop superconducting structures, including different sized loops, varying degrees of target-loop overlap, and even the interesting prospect of flux pumping stacks of superconducting structures (similar to [27]), would be an important and useful extension to the worked discussed in this article.

The ability to account for cross-talk between neighbouring superconducting loops is a significant advancement towards the realisation of a planar, persistent-current magnetic field source for the Geonium Chip Penning trap. It means that the flux pumping scheme outlined in [21] can be applied to more than one structure while still allowing for complete control of the magnetic field distribution. Flux pumping therefore remains a promising method of operating the new magnetic field source of the Geonium Chip. While the motivation for this work has been for an ion trap experiment, we believe the techniques outlined here could be useful for other quantum systems relying on precise control of stable magnetic field distributions, particularly in applications where portability and scalability are important.

ACKNOWLEDGMENT

The authors would like to thank all group members of the Geonium Chip Group at the University of Sussex for their contributions.

REFERENCES

[1] T.D. Ladd, F. Jelezko, R. Laflamme, Y. Nakamura, C. Monroe, and J. L. O'Brien, "Quantum Computers," *Nature*, vol. 464, no. 7285, pp. 45-53, March 2010.

[2] J.P. Home, D. Hanneke, J.D Jost., J.M. Amini, D. Leibfried, and D.J. Wineland, "Complete methods set for scalable ion trap quantum information processing," *Science*, vol. 325, no. 5945, pp. 1227-1230, Aug. 2009.

[3] M.J. Madsen, W.K. Hensinger, D. Stick, J.A. Rabchuk, and C. Monroe, "Planar ion trap geometry for microfabrication,", *Appl. Phys. B*, vol. 78, no. 5, pp. 639-651, Mar. 2004.

[4] R. Folman, P. Krüger, J. Schmiedmayer, J. Denschlag, and C. Henkel, "Microscopic atom optics: from wires to an atom chip,", *Adv. in At. Mol. Opt. Phys.*, vol. 48, no. C, pp. 263-356, Jan. 2002.

[5] M. Keil, O. Amit, S. Zhou, D. Groswasser, Y. Japha, and R. Folman, "Fifteen years of cold matter on the atom chip: promise, realizations, and prospects," *J. Mod. Opt.*, vol. 63, no. 18, pp. 1840-1883, Oct. 2016.

[6] M.F. Riedel, P. Böhl, Y. Li, T.W. Hänsch, A. Sinatra, P. Treutlein, "Atom-chip-based generation of entanglement for quantum metrology," *Nature*, vol. 464, no. 7292, pp. 1170-1173, Apr. 2010.

[7] Y. Margalit, O. Dobkowski, Z. Zhou, O. Amit, Y. Japha, S. Moukouri, D. Rohrlich, A. Mazumdar, S. Bose, C. Henkel, and R. Folman, "Realization of a complete Stern-Gerlach interferometer: Toward a test of quantum gravity," *Sci. Adv.*, vol. 17, no. 22, May 2012.

[8] J. Verdú, "Theory of the coplanar-waveguide Penning trap," *New J. Phys.*, vol. 13, no. 11, Nov. 2011, Art. ID. 113029.

[9] J. Pinder and J. Verdú, "A planar Penning trap with tunable dimensionality of the trapping potential," *Int. J. Mass Spectrom.*, vol. 359, no. 49, pp. 49-56, Dec. 2013.

[10] J. Verdú, "Ion trap", U.S. Patent 8,362,423 B1, Jan. 29, 2013.

[11] J. Verdú, "Ion trap", Intl. Patent No. WO 2013/041615 A2, Mar. 28, 2013.

[12] A. Cridland, J.H. Lacy, J. Pinder, and J. Verdú, "Single microwave photon detection with a trapped electron," *Photon.*, vol. 3, no. 4, p. 59, Nov. 2016.

[13] A. Cridland Mathad, J.H. Lacy, J. Pinder, A. Uribe, R. Willetts, R. Alvarez, and J. Verdú, "Coherent coupling of a trapped electron to a distant superconducting microwave cavity," *Appl. Phys. Lett.* vol. 117, no. 15, Oct. 2020, Art. ID. 154001.

[14] F. Crimin, I. Marzoli and J. Verdú, "Quantum Illumination in the Geonium Chip, a feasibility study," Confidential report for Leonardo MW Ltd. Funded under private research contract #4500138590 / University of Sussex, 2018.

[15] W. Jhe, D. Phillips, L. Haarsma, J. Tan, and G. Gabrielse, "Cylindrical Penning Traps and Self-Shielding Superconducting Solenoids for High Precision Experiments," *Phys. Scr.*, vol. 46, no. 3, pp. 264-267, Sep. 1992.

[16] G. Gabrielse and J. Tan, "Self-Shielding Superconducting Solenoid Systems," *J. Appl. Phys.*, vol. 63, no. 10, pp. 5143-5148, May 1988.

[17] D. Park, J. Lee, J. Bascuñan, P.C. Michael, and Y. Iwasa, "HTS Shim Coils Energized by a Flux Pump for the MIT 1.3-GHz LTS/HTS NMR Magnet: Design, Construction, and Results of a Proof-of-Concept Prototype," *IEEE Trans. Appl. Supercond.*, vol. 28, no. 3, Apr. 2018, Art. ID. 4301105.

[18] J. Reichel, "Microchip traps and Bose-Einstein condensation,", *Appl. Phys. B*, vol. 75, no. 6, pp. 469-487, Apr. 2002.

[19] J. Pinder, J.H. Lacy, R. Willetts, A Cridland Mathad, A. Uribe, and J. Verdú, "Planar, strong magnetic field source for a chip ion trap," *Rev. Sci. Instrum.*, vol. 91, no. 10, Oct. 2020, Art. ID. 103201.

[20] J. H. Lacy, "Development of a planar magnetic field source for the Geonium Chip Penning Trap," Doctoral dissertation, University of Sussex, Falmer, UK, 2019.

[21] J.H. Lacy, A. Cridland, J. Pinder, A. Uribe, R. Willetts and J. Verdú, "Superconducting Flux Pump for a Planar Magnetic Field Source," in *IEEE Trans. Appl. Supercond.*, vol. 30, no. 8, pp. 1-12, Dec. 2020, Art. ID. 4902412.

[22] H. Dehmelt, "Continuous Stern-Gerlach effect: Principle and idealized apparatus," *Proc. Natl. Acad. Sci. USA*, vol. 83, no. 8, pp. 2291-2294, Apr. 1986.

[23] L.D. Landau and E.M. Lifshitz, "Electrodynamics of Continuous Media", vol. 8 (Oxford:Pergamon), section 42, 1960.

[24] L. J. M. van de Klundert, and H. H. J. ten Kate, "Fully superconducting rectifiers and flux pumps Part 1: Realized methods for pumping flux," *Cryogenics*, vol. 21, no. 4, pp. 195-206, Apr. 1981.

[25] T.A. Coombs, J. Geng, L. Fu, and K. Matsuda, "An Overview of Flux Pumps for HTS Coils," *IEEE Trans. Appl. Supercond.*, vol. 27, no. 4, Jun. 2017, Art. ID. 4600806.
[26] G.A. Levin, P.N Barnes, J. Murphy, L. Brunke, J.D. Long, J. Horwath, and Z. Turgut, "Persistent current in coils made out of second generation high temperature superconductor wire," *Appl. Phys. Lett.* vol. 93, no. 6, Aug. 2008, Art. ID. 062504.
[27] H. Zhang *et al.*, Magnetization of HTS Coated Conductor Stacks Using Flux Pumping, *IEEE Trans. Appl. Supercond.*, vol. 27, no. 4, Jun. 2017, Art. ID. 8200205.